

Nodes and Spin Windings for Topological Transitions in Light-Matter Interactions: Anisotropic Quantum Rabi Model as a Born Abstract Artist

Zu-Jian Ying^{1,*}

¹*School of Physical Science and Technology, Lanzhou University, Lanzhou 730000, China*

By extracting different levels of topological information a new light is shed on the energy spectrum of the anisotropic quantum Rabi model (QRM) which is the fundamental model of light-matter interactions with indispensable counter-rotating terms in ultra-strong couplings. Besides conventional topological transitions (TTs) at gap closing, abundant unconventional TTs including a particular one universal for different energy levels are unveiled underlying level anticrossings without gap closing by tracking the wave-function nodes. On the other hand, it is found that the nodes have a correspondence to spin windings, which not only endows the nodes a more explicit topological character in supporting single-qubit TTs but also turns the topological information physically detectable. Furthermore, hidden small-spin-knot transitions are exposed for the ground state, while more kinds of spin-knot transitions emerge in excited states including unmatched node numbers and spin winding numbers. As a surprise, frequently the spin windings produce portraits in high spiritual similarity with abstract artistic works, which demonstrates that the anisotropic QRM may be the Picasso of physical models. This signifies that art is joining the dialogue between mathematics and physics which was triggered by the milestone work of revealing integrability of the QRM.

PACS numbers:

I. INTRODUCTION

Among the intensive dialogue between mathematics and physics¹⁻⁶⁰ triggered by the milestone work of D. Braak who revealed the integrability of the quantum Rabi model (QRM),¹ few-body quantum phase transitions (QPTs) have recently attracted a special attention in the context of light-matter interactions.^{4,13-23} In reality, the continuing experimental enhancements of couplings have brought the era of ultra-strong^{5,6,61-70} and even deep-strong couplings,^{70,71} which makes few-body QPTs practically relevant. Along with the applications of few-body QPTs e.g. in critical quantum metrology,³²⁻³⁵ single-qubit topological phase transitions have also added an interesting topic in the mathematics-physics dialogue with a renewed insight for the transitions in light-matter interactions.¹⁹⁻²¹

In the QRM,^{24,72} which is a most fundamental model of light-matter interactions, the QPT¹³⁻¹⁵ occurs in the low frequency limit, that is, $\omega/\Omega \rightarrow 0$ where ω is the bosonic frequency and Ω is the atomic level splitting or tunneling strength, which is a replacement of thermodynamical limit in condensed matter. Although whether the transition should be termed quantum or not might be a matter of taste due to the negligible quantum fluctuations in the photon vacuum state,¹¹ it has been established that the critical exponents of the single-qubit QRM can be bridged to the thermodynamical case.¹⁶ Indeed, the photon number has a superradiant-like behavior^{13,14,19,21} as experimentally observed⁷³⁻⁷⁵ in the Dicke model which is a thermodynamical version of the QRM. Moreover, when universality is a character born with

QPT,^{11,76} the QPT of QRM manifests a universal critical scaling relation with respect to the anisotropy of linear coupling,^{16,19,21} and more robust scaling relations can be found in the presence of nonlinear coupling.²¹ Despite of the preserved parity symmetry in the Hamiltonian of the QRM, such a QPT has a hidden symmetry breaking¹⁹ in the ground state as in the traditional Landau class of phase transitions.

Away from the low frequency limit, the aforementioned critical universality however collapses at finite frequencies.^{19,21} Surprisingly, in such a diversified situation⁷⁷ another universality classification can be found from the common node numbers of the ground-state wave functions, which reveals the topological nature of the emerging series of transitions with symmetry protection, essentially different from the Landau class of phase transitions.¹⁹⁻²¹ Such topological transitions (TTs) are usually conventional ones with gap closing as those in condensed matter,⁷⁸⁻⁸⁴ while unconventional ones without gap closing also exist²⁰ analogously to the unconventional cases in the quantum spin Hall effect with strong electron-electron interactions⁸⁵ and the quantum anomalous Hall effect with disorder.⁸⁶ The topological classification applies not only for linear couplings but also for the nonlinear Stark interaction.²¹ While nodes of wave functions are the center of Feynman's node theorem which generally governs one-dimensional confined spinless systems,⁸⁷ it is demonstrated that the ground state of the QRM also obeys the no-node theorem.²⁰ Nodes of polynomial functions are related to topological Galois theory in connecting algebra to topology.⁸⁸ The node number can be used to distinguish topological difference of quantum states in the sense that by fixing a node number one cannot go to another node state by continuous shape deformation of the wave function, just as one cannot change a torus into a sphere by a continuous deformation. Be-

* yingzj@lzu.edu.cn

sides such a topological picture as in so-called rubber-sheet geometry, one may be wondering if there is any more physical demonstration for the topological connection of nodes in wave functions.

On the other hand, for the light-matter interaction it has been shown that it is necessary to take the counter-rotating terms (CRTs) into account²⁷ to fit the experimental energy spectrum in ultra-strong couplings.⁶¹ In fact, the anisotropy describing the CRTs is an important parameter in experiments which is highly controllable.⁸⁹ In the absence of the CRTs the system denoted by the Jaynes-Cummings model (JCM)⁹⁰ possesses symmetries of the excitation number and momentum-position duality.^{19,54} The CRTs break both the symmetries including the U(1) symmetry so that the excitation number is not longer a good quantum number, while the emerging level anticrossings (also called avoided crossings) lead to a different energy spectrum. Although the Z_2 symmetry of parity is preserved in the presence of the CRTs, the parity is not enough at all to label the various quantum states. It has been shown that level crossings occur on the so-called ‘‘baselines’’ in coupling variation,⁵⁴ while it is not clear what is really happening to the quantum states during level crossings and anticrossings. The aforementioned node number has been applied for a renewed classification of the ground state,^{19–21} however it is still unexplored for the excited states which may have different scenarios. In such a situation, a full identification and a complete understanding for all quantum states in the presence of the CRTs are still lacking even when the QRM has been long studied for over eight decades.^{24,72}

Conventionally in condensed matter topological phases are concerning about the ground state,⁹¹ while for the ground state single-qubit systems in light-matter interactions also have analogs of TTs.^{19–21} Since state occupation of single-qubit systems only involves a single eigenstate which is free of filling problem in condensed matter with Fermi level, to get some topological insight for the energy spectrum we can extend the exploration of TTs to excited states. In the present work, we provide a topological point of view for the energy spectrum of the anisotropic QRM. We find that not only the level crossings but also the level anticrossings are associated with TTs as tracked by the node number of the eigenstate wave function. On the other hand, we show that the nodes of the wave function corresponds to the zeros of spin windings, which endows nodes an explicit topological character and provides a more solid support for single-qubit TTs. In such a topological classification, the spin winding direction contributes an additional quantum feature for a full identification of various ground states. For the excited states, apart from the TTs associated with level crossing or anticrossing, novel TTs with unmatched node numbers and winding numbers also emerge due to anti-winding large spin knots. A more extensive investigation on spin knots reveals hidden small-knot transitions for the ground state and more kinds of spin-knot transitions for the excited states. Our study

extracts different levels of topological information, from wave-function topology to spin-winding topology, with exploration from one-axis nodes to two-axis nodes and in the absence or presence of various spin knots including small, big, huge and diagonal ones. The abundant topological information may renew our knowledge about the underlying variation of the quantum states in light-matter interactions. Besides the unveiled variety of novel TTs, a surprising finding is that the figures produced by the spin windings frequently resemble various portraits as in abstract artistic works in such an amazing spiritual similarity that we believe the anisotropic QRM is a born abstract artist.

The paper is organized as follows. Section II introduces the anisotropic QRM which is a fundamental model describing light-matter interactions with the CRTs. Section III illustrates the energy spectrum with level crossing and anticrossings. Section IV unveils underlying TTs of node numbers around the anticrossings and an unconventional TT universal for different states. The correspondence of nodes and spin windings is shown in Section V, which yields a full topological classification including winding directions for the ground state. Section VI reveals new TTs with unmatched node numbers and winding numbers in the excited states. Section VII gives node sorting and algebraic formation for spin winding number, which inspires and facilitates the exploration of the transitions of different spin knots in Section VIII. Section IX is devoted to conclusions and discussions.

II. MODEL AND SYMMETRY

The continuing experimental progresses in enhancing the strength of light-matter interactions have brought us to the era of ultra-strong^{5,61–70} and even deep-strong couplings,^{70,71} with the ratio of the coupling strength and the bosonic frequency going beyond 0.1 and 1.0 respectively. In such coupling regimes, the CRTs play an indispensable role, as shown by the Bloch-Siegert shift^{61,92} and the fitting²⁷ of the experimental spectra.⁶¹ Indeed the CRTs are controlled by the coupling anisotropy ratio λ , while recently a very wide strength range of anisotropy ratios from $\lambda = 0.2$ to $\lambda = 2.88$ have been experimentally tuned to.⁸⁹ Access to ultra-strong couplings can be also possible for $\lambda = 0$ in circuit-QED systems.^{93,94} In such a situation, the anisotropic coupling is described by the anisotropic QRM of which the Hamiltonian reads

$$H = \omega a^\dagger a + \frac{\Omega}{2} \sigma_x + g [(\tilde{\sigma}_- a^\dagger + \tilde{\sigma}_+ a) + \lambda (\tilde{\sigma}_+ a^\dagger + \tilde{\sigma}_- a)]. \quad (1)$$

Here ω is the frequency of a bosonic mode created (annihilated) by a^\dagger (a) and $\sigma_{x,y,z}$ are the Pauli matrices. The anisotropy ratio λ tunes the afore-mentioned CRTs which, along with the rotating-wave terms, contribute to the total coupling with strength g . Following refs.^{10,14} we have used the spin basis $\sigma_z = \pm$ which conveniently represents the two flux states in the flux-qubit circuit

systems,⁹⁵ with an unconventional definition of spin raising and lowering operators $\tilde{\sigma}^{\pm} = (\sigma_z \mp i\sigma_y)/2$. Nevertheless, the conventional form of the QRM ($\lambda = 1$) can be retrieved by a spin rotation $\{\sigma_x, \sigma_y, \sigma_z\} \rightarrow \{\sigma_z, -\sigma_y, \sigma_x\}$ around the axis $\vec{x} + \vec{z}$. The Ω term denotes the atomic level splitting in cavity systems and tunneling^{10,14} in flux-qubit circuit systems.

We transform into the effective spatial space

$$H = \frac{\omega}{2}\hat{p}^2 + v_{\sigma_z}(x) + \left[\frac{\Omega}{2} - g_y i\sqrt{2}\hat{p}\right]\sigma^+ + \left[\frac{\Omega}{2} + g_y i\sqrt{2}\hat{p}\right]\sigma^- \quad (2)$$

by the quadrature representation, $a^\dagger = (\hat{x} - i\hat{p})/\sqrt{2}$, $a = (\hat{x} + i\hat{p})/\sqrt{2}$, with momentum $\hat{p} = -i\frac{\partial}{\partial x}$. Now $\sigma_x = \sigma^+ + \sigma^-$, $\sigma_y = -i(\sigma_+ - \sigma_-)$ are the conventional forms of spin raising and lowering on the $\sigma_z = \pm$ basis. The effective harmonic potentials $v_{\sigma_z}(x) = \omega(x + g'_z\sigma_z)^2/2 + \varepsilon_0^z$ include a spin-dependent displacement $g'_{y,z} = \sqrt{2}g_{y,z}/\omega$, where $g_y = \frac{(1-\lambda)}{2}g$ and $g_z = \frac{(1+\lambda)}{2}g$, and a constant shift $\varepsilon_0^z = -\frac{1}{2}[g_z'^2 + 1]\omega$. The g_y term can be written as $\sqrt{2}g_y\hat{p}\sigma_y$ which resembles the Rashba spin-orbit coupling in nanowires⁹⁶⁻¹⁰⁰ or the equal-weight mixture^{101,102} of the linear Dresselhaus ($\hat{p}_x\sigma_y + \hat{p}_y\sigma_x$) and Rashba ($\hat{p}_x\sigma_y - \hat{p}_y\sigma_x$) spin-orbit couplings in condensed matter^{103,104} and cold atomic gases.^{101,102,105} We will analyze by standing in positive- λ regime and x space while the picture for negative- λ regime is similar in p space under the x - p duality transformation $\{\sigma_x, \sigma_y, \sigma_z\} \rightarrow \{\sigma_x, -\sigma_z, \sigma_y\}$, $x \rightarrow p$, $\lambda \rightarrow -\lambda$.¹⁹⁻²¹

The model at any anisotropy has the parity symmetry, $[\hat{P}, H] = 0$ with $\hat{P} = \sigma_x(-1)^{a^\dagger a}$ which includes simultaneously the spin reversion and the space inversion $x \rightarrow -x$.^{18,19} The parity not only impose the symmetry on the wave function but also leads to symmetric/antisymmetric spin textures as addressed later on.

III. LEVEL ANTI-CROSSINGS IN ENERGY SPECTRUM

An illustration of the energy spectrum is presented in **Figure 1**, where the levels with a negative (positive) parity are plotted by blue solid (red dotted) lines. One sees in **Figure 1a** that in the presence of the CRTs ($\lambda \neq 0$) the energy levels exhibit level crossings between states with opposite parities, while level anticrossings occur between states with same parities. In contrast, there is no anticrossing in the absence of the CRTs ($\lambda = 0$) as in **Figure 1b**.

The full level crossings at $\lambda = 0$ are results of the symmetries of the JCM which preserves the parity, the excitation number and the position-momentum duality.^{19,20,54} However, the symmetries of the excitation number and the position-momentum duality are broken once the CRTs are introduced, which is the origin of the level anticrossings. Nevertheless the symmetry of parity is still preserved, which partially keeps level crossings. In fact, both the JCM part and the CRTs commute with the

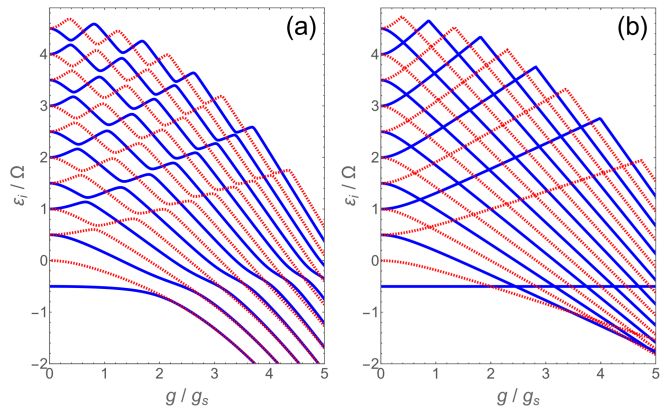


FIG. 1. Level crossing and anticrossings in the energy spectrum ε_i at fixed anisotropy: (a) $\lambda = 0.5$, (b) $\lambda = 0.0$. Here $i = j_E = 1, 2, \dots$ labels the energy levels from the ground state to excited states. The blue solid (red dotted) lines represent levels in positive (negative) parity. All figures are illustrated at $\omega = 0.5\Omega$ throughout the paper.

parity operator. Around the level anticrossings the CRTs mix the crossing states with a same parity in the absence of the CRTs, which opens a gap. However, around the level crossings such a state mixing is excluded as any combination of states with opposite parities would break the parity symmetry thus violating the conditions for eigenstates.

Despite that the energy spectrum is known, one can never say the physics behind has been fully explored. In the following we will provide some novel insights for the level crossings and anticrossings from topological point of view.

IV. NODE FEATURE FOR TOPOLOGICAL CLASSIFICATION

A. Transitions of Wave-Function Node Status in Level Crossings and Anticrossings

To find out the possible transitions of quantum states around the level crossings and anticrossings, we monitor the wave function in continuous variation of a system parameter. As mentioned in Introduction, in the low-frequency limit the ground state of the generalized QRM with anisotropy^{16,19-21} and nonlinear Stark coupling²¹ can exhibit critical universality which however breaks down at finite frequencies.^{19,21} Nevertheless, in the breaking down of the critical universality another class of universality, namely topological universality, can be found from the common feature of node number of the ground-state wave function.¹⁹⁻²¹ As one knows a common example of a topological invariant is the number of holes in an object, here the topological invariant is the number of nodes in a ground-state wave function. We find such topological classification also applies for excited states

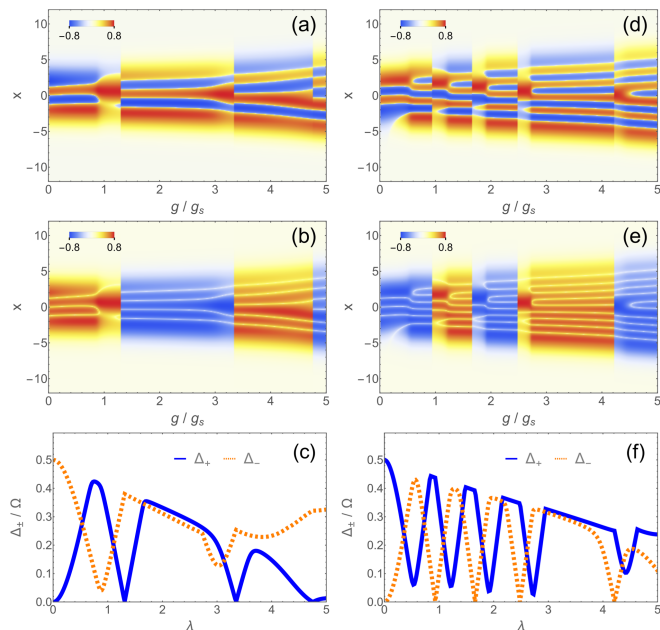


FIG. 2. Connection of level crossing and anticrossing with topological transitions in variation of coupling g , at fixed $\lambda = 0.2\Omega$ for $j_E = 5$ (a-c) and fixed $\lambda = 0.3\Omega$ for $j_E = 10$ (d-f). (a,d) $\psi_+(x)$, (b,e) $\psi_+^*(x) \times \psi_-(-x)$, (c,f) Δ_{\pm} . The plot amplitude is amplified e.g. by $|\psi_{\pm}|^{1/4}$ to increase the color contrast.

and can provide a novel view for the level crossings and anticrossings.

The nodes are defined as the zeros of wave function which are decided by

$$\psi_+(x_Z) = P\psi_-(-x_Z) = 0, \quad (3)$$

under parity value $P = \pm 1$, while the node number n_Z counts the node pairs $\pm x_Z$ totally in ψ_{\pm} . **Figure 2a,d** show the wave function in spin-up component $\psi_+(x)$ versus the increase of the coupling g , with blue (red) color representing negative (positive) values, while the nodes appear as the red/blue boundaries. **Figure 2b,e** denote the product of the wave-function components,

$$\psi_+^*(x)\psi_-(-x) = P|\psi_+(x)|^2, \quad (4)$$

which indicates a negative (positive) parity in blue (red) while the track of a node appears as a white line. **Figure 2c,f** depict the upper gap Δ_+ (lower gap Δ_-) by the blue solid (orange dotted) lines, with vanishing value marking a level crossing and finite dip displaying an anticrossing.

Figure 2a-c illustrate the case for the fifth excited states ($j_E = 5$). As expected, the level crossings are always accompanied with transitions of both parity and node number, as the transitions around $g = 1.3g_s$ and $g = 3.4g_s$. The situation is different for a level anticrossing as there is no parity reversal while there are still transitions of node number for a small anticrossing gap, as in

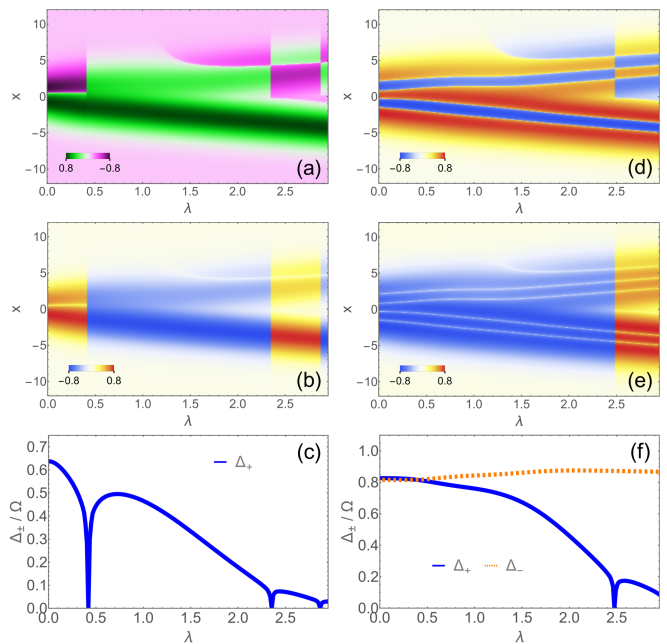


FIG. 3. An unconventional TT without gap closing universal for different eigenstates beyond $\lambda = 1$, illustrated for $j_E = 1$ (a-c) and $j_E = 5$ (d-f) at fixed $g = 2.2\Omega$ and $\omega = 0.5\Omega$. (a,d) $\psi_+(x)$, (b,e) $\psi_+^*(x) \times \psi_-(-x)$, (c,f) Δ_{\pm} .

the example around $g = 0.9g_s$ in **Figure 2a-c**. For a larger anticrossing gap, as in the case around $g = 3g_s$, one can still see the tendency of node modification despite that a final transition is not triggered. Note that conventionally TTs occur with gap closing,^{19,78–81} as those at level crossings. The TTs here around level anticrossings are *unconventional* ones in the sense that they occur without gap closings,^{20,85,86} since both upper and lower gaps are finite at the transitions. The unconventional TTs around level anticrossings become more popular in higher excited states as illustrated by $j_E = 10$ in **Figure 2d-f** where level crossings and anticrossings emerge more frequently.

B. An Unconventional Topological Transition Universal for Different Eigenstates

When we vary the anisotropy, level crossings and anticrossings can also occur similarly. Here, it is worthwhile to pay attention to a special TT, as in **Figure 3** around $\lambda = 1.1$, which turns out to be quite particular with the following special features together: (i) This transition is unconventional one without gap closing or parity reversal, as demonstrated in **Figure 3a,b,d,e**. (ii) Although this transition occurs in gapped situation, it seems to be not associated with level anticrossing, as indicated by the dotted line in **Figure 3f** which is flat and shows no sign of level anticrossing. (iii) While the variation of node number occurs usually around the origin position, the new node for this transition is coming from the infinity side, as shown **Figure 3a,d**. (iv) This transition is universal for

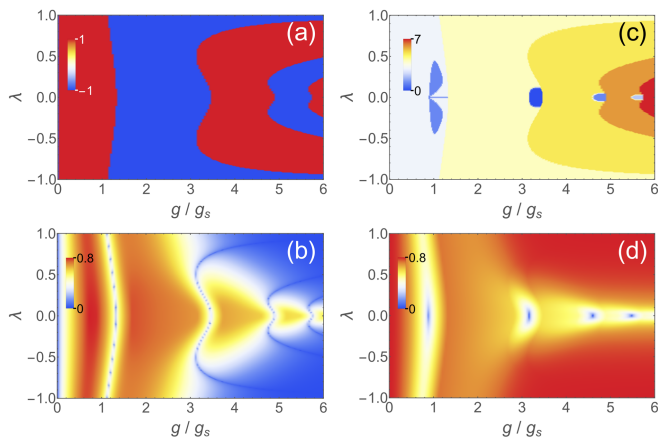


FIG. 4. Phase diagrams in g - λ plane for $j_E = 5$. (a) Parity P , (b) Upper gap Δ_+/Ω , (c) Node number n_Z , (d) Lower gap Δ_-/Ω .

different eigenstates, as illustrated for $j_E = 1, 5$ in Figure 3a,d. This transition should originate from the sign reversal of g_y which changes the energy competitions for the Rashba spin-orbit term without changing the parity.²⁰ Of course, for this g_y -sign reversal to come to final effect it has to overcome the resistance from the other terms in kinetic, potential, and tunneling parts as in (2). As the node in this transition is introduced from the infinity side, the state-dependent parity is not affected and different states have similar wave-function profiles which are all decaying away from the main wave packets around the origin. Thus, the g_y -sign reversal is facing an energy competition situation similar for different states, this may be the reason why this transition is universal.

This particular transition may have some special advantages. The gapped situation in feature (i) avoids the detrimental slowing-down effect close to a critical point with vanishing gap in preparing probe state if it is used for some quantum sensors or devices.³⁵ The feature (ii) ensures a large gap, since otherwise level anticrossings have finite but small gaps. The feature (iii) will not reverse the parity thus will not introduce a level crossing or gap closing.²¹ The feature (iv) breaks the limitation of ground state so that eigenstates have the same transition, which could provide great convenience in case the ground state is difficult to reach. Moreover, the transition can occur in all coupling regimes as one will see in Figure 8 and Figure 9c.

C. Phase Diagrams of Parity, Gaps and Nodes

To have an overall view for the connection of the level crossings/anticrossings and the TTs, we present the phase diagrams of parity, gaps and nodes in g - λ plane in **Figure 4** for $j_E = 5$ and **Figure 5** for $j_E = 11$. In Figure 4, the parity reversal (panel (a)) occurs with upper gap closing (panel (b)) at the main phase boundaries in

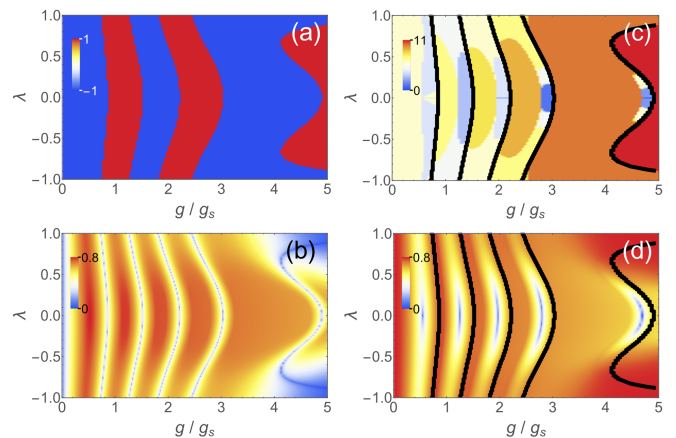


FIG. 5. Phase diagrams in g - λ plane for $j_E = 11$. (a) Parity P , (b) Upper gap Δ_+/Ω , (c) Node number n_Z , (d) Lower gap Δ_-/Ω . The black solid lines in (c,d) mark the level crossing boundaries in (a,b).

the node phase diagram (panel (c)). The level anticrossings take place apart from but nearby the level crossing boundaries, as indicated by small lower gap Δ_- depicted by blue color in panel (d). The anticrossing effect is weaker at larger couplings around $g = 3.1, 4.6, 5.5g_s$, as one sees that the small- Δ_- regions (blue) are narrow and only limited to the vicinity of $\lambda = 0$, correspondingly the unconventional TTs with node-number variations in Figure 4c occur also around these narrow regions in Figure 4d. The level anticrossing effect is relatively stronger around $g = 0.9g_s$ as the regime with the small lower gap is more extended along λ direction, while the transitions in node number appear also in a wider regime. For a higher excited state, as $j_E = 11$ in Figure 5, the regimes of effective anticrossings are much extended for large couplings, correspondingly the unconventional TTs merge in larger values of λ , as one sees in panels (c) and (d).

The above analysis on the excited states also provides some more insight for the ground state. The phase diagrams of parity, gaps and nodes for the ground state have been established in refs.^{19,20}, as also will be re-classified in Section V E of the present work after finding the correspondence of nodes to the spin windings. What relevant here is the feature that the TTs in the ground state are purely conventional ones except the particular unconventional TT above $\lambda = 1$ addressed in Section IV B. The pure conventional TTs demonstrate that, as far as the ground state is concerned, the anisotropic QRM and the JCM topologically belong to the same class. This unification in some sense makes up for the loss in the symmetry breaking of excitation number and position-momentum duality^{19,21} which have disconnected the JCM and the anisotropic QRM in the scaling relation in critical universality classification.^{16,19,21} Now with the above analysis on the level anticrossings, we gain a further understanding for the origin of the pureness of topological phase transitions in ground states: there is no anticrossing ef-

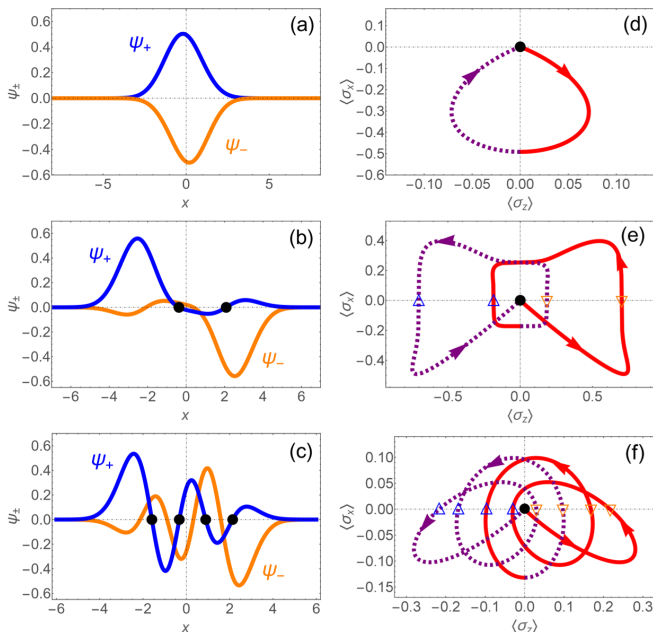


FIG. 6. Correspondence of nodes and spin windings in $0 \leq \lambda < 1$ regime: Wave function $\psi_{\pm}(x)$ (a-c) and spin winding (d-f) of the ground state ($j_E = 1$) at $g = 1.5g_s$ (a,d), the ground state at $g = 4.4g_s$ (b,e), and the fifth state ($j_E = 5$) at $g = 1.5g_s$ (c,f). The dots in (a-c) mark the nodes in $\psi_+(x)$. The dots in (d-f) locate the origin in $\langle\sigma_z\rangle$ - $\langle\sigma_x\rangle$ plane, the upward (downward) triangles label the nodes in $\psi_+(x)$ ($\psi_-(x)$), and the arrows indicates the winding direction. The $x < 0$ ($x > 0$) regime is plotted by solid (dotted) line in (d-f) and the spin-expectation amplitudes are plotted by $|\sigma_i|^{1/4}$ in (e) for a better visibility. Here $\lambda = 0.2$ for all panels.

fect for the ground state as the only gap is the upper gap which solely involves level crossings.

V. SPIN WINDINGS FOR TOPOLOGICAL FEATURE

The wave-function nodes might remind one of one-dimensional confined spinless systems, the ground states of which however never have transition of nodes due to the constraint of the no-node theorem.⁸⁷ Now that we also extend the discussion of TTs to excited states, we should bring more attention to the fact that differently from the spinless systems our systems involve the spin nontrivially, especially the g_y term resembles the Rashba/Dresselhaus spin-orbit coupling while spin-orbit coupling is often fundamentally responsible for TTs in condensed matter.^{79,80,96–98,100}

In this section we shall look at the spin texture in the position space which will upgrade the topological information from the wave function level to physical observ-

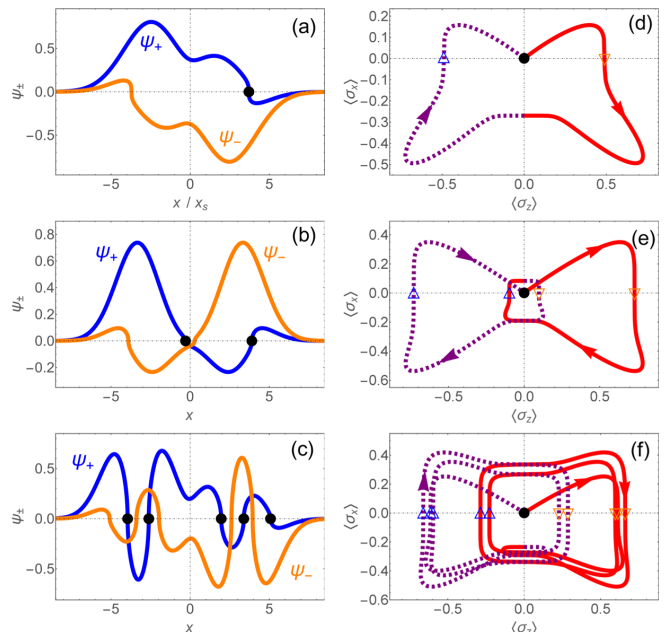


FIG. 7. Correspondence of nodes and spin windings in $\lambda > 1$ regime: Wave function $\psi_{\pm}(x)$ (a-c) and spin winding (d-f) of the ground state at $\lambda = 2.0$ (a,d), the ground state at $\lambda = 3.0$ (b,e), and the fifth state at $\lambda = 3.0$ (c,f), with the symbols as in Figure 6. The plot amplitudes are amplified by $|\psi_{\pm}|^{1/3}$ in (a), $|\psi_{\pm}|^{1/2}$ in (b,c), $|\sigma_i|^{1/4}$ in (d,f) and $|\sigma_i|^{1/5}$ in (e). Here $g = 1.7g_s$ for all panels.

able level. The spin texture can be extracted by

$$\langle\sigma_z(x)\rangle = \psi_+^*(x)\psi_+(x) - \psi_-^*(x)\psi_-(x), \quad (5)$$

$$\langle\sigma_x(x)\rangle = \psi_+^*(x)\psi_-(x) + \psi_-^*(x)\psi_+(x), \quad (6)$$

$$\langle\sigma_y(x)\rangle = i[\psi_-^*(x)\psi_+(x) - \psi_+^*(x)\psi_-(x)], \quad (7)$$

which are instantaneous spin expectations at position x . Note that, as shown in Figure 1, the eigenstates are all non-degenerate except at the crossing points, so that the eigenfunctions can be chosen to be all real, i.e.

$$\psi_{\pm}^*(x) = \psi_{\pm}(x), \quad (8)$$

which is also valid even at the crossing points if one is not mixing up different parity states. From the spin texture we will see the correspondence of wave-function nodes and spin windings for the ground state and find more hidden TTs in excited states.

A. Constraints of the Parity Symmetry on Spin Texture

As afore-mentioned, the wave-function components in opposite spins are related by $\psi_-(x) = P\psi_+(-x)$ due to the parity symmetry. As a consequence, $\langle\sigma_y\rangle$ is always vanishing,

$$\langle\sigma_y(x)\rangle = iP[\psi_+(-x)\psi_+(x) - \psi_+(x)\psi_+(-x)] = 0. \quad (9)$$

and the spin evolution lies only in $\langle\sigma_z\rangle$ - $\langle\sigma_x\rangle$ plane. Besides the vanishing $\langle\sigma_y(x)\rangle$, the parity symmetry also leads to symmetric $\langle\sigma_x(x)\rangle$ and antisymmetric $\langle\sigma_z(x)\rangle$,

$$\langle\sigma_x(-x)\rangle = \langle\sigma_x(x)\rangle, \quad \langle\sigma_z(-x)\rangle = -\langle\sigma_z(x)\rangle, \quad (10)$$

which hold for both parity values $P = \pm 1$, as one can see directly from Equations (5) and (6).

B. Correspondence of Wave-Function Nodes and Spin-Winding Zeros

We find the evolution of $\langle\sigma_z\rangle$ and $\langle\sigma_x\rangle$ with respect to x forms spin windings in $\langle\sigma_z\rangle$ - $\langle\sigma_x\rangle$ plane, as shown in **Figure 6** where the wave functions are shown in panels (a-c) while the corresponding spin windings are displayed in panels (d-f). At a small coupling where the wave function of the ground state has no node in panel (a), also the spin winding does not effectively surround the origin (black dot) in panel (d). At a larger coupling in panel (b) the wave function has two nodes as marked by the black dots for ψ_+ , the spin in panel (e) is really winding around the origin with two pairs of zeros of $\langle\sigma_x\rangle$ respectively corresponding to the nodes in ψ_+ (upward triangles) and ψ_- (downward triangles). Similar spin windings can be seen for the excited states as shown in panels (c,f) where more nodes are formed with more spin windings correspondingly.

The correspondence of wave-function nodes and spin-winding zeros can be seen from Equations (3) and (6) which always assign a vanishing value to $\langle\sigma_x(x)\rangle$

$$\langle\sigma_x(x_Z)\rangle = 0 \quad (11)$$

at a wave-function node x_Z defined in (3). Reversely a zero of $\langle\sigma_x(x)\rangle$ also requires the node of wave function as

$$\langle\sigma_x(x)\rangle = 2\psi_+(x)\psi_-(x) = 2P\psi_+(x)\psi_+(-x). \quad (12)$$

Any finite coupling will lead to a displacement in $v_{\sigma_z}(x)$ and break the space-inversion symmetry (without spin reversal), thus in principle one will not have negative-positive symmetric nodes within a same component of wave function like $\psi_+(x_Z) = \psi_+(-x_Z) = 0$ which otherwise would have two nodes of $\psi_+(x)$ simultaneously correspond to one $\langle\sigma_x(x)\rangle$ zero. In the absence of coupling one has such negative-positive symmetric nodes, however even in such symmetric cases $-x_z$ by parity symmetry is also the node of $\psi_-(x)$ which avoids the double counting of the total node number in ψ_{\pm} . That is to say, the total node number in ψ_{\pm} is still equal to the total zero number of $\langle\sigma_x(x)\rangle$. So we can conclude that the wave-function nodes of ψ_{\pm} and the $\langle\sigma_x(x)\rangle$ zeros are one-to-one corresponding by total number or by pair number. Thus, the wave-function nodes can be detected by the zeros of $\langle\sigma_x(x)\rangle$, which turns the topological information to be measurable.

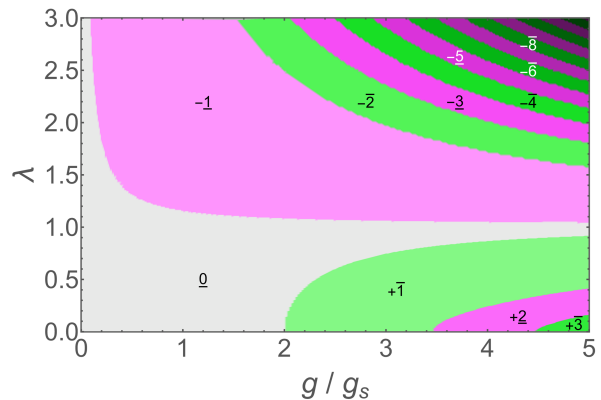


FIG. 8. Spin winding direction and a full classification in topological phase diagram of ground state. The number represents the node number or the spin winding number with the positive (negative) sign labeling counterclockwise (clockwise) winding direction, while the overline (underline) denotes positive (negative) parity.

C. Spin Winding Number

One can estimate the rounds of spin winding by the winding number around the origin in the $\langle\sigma_z\rangle$ - $\langle\sigma_x\rangle$ plane as calculated by

$$n_{zx} = \frac{1}{2\pi} \int_{-\infty}^{\infty} \frac{\langle\sigma_z(x)\rangle\partial_x\langle\sigma_x(x)\rangle - \langle\sigma_x(x)\rangle\partial_x\langle\sigma_z(x)\rangle}{\langle\sigma_z(x)\rangle^2 + \langle\sigma_x(x)\rangle^2} dx, \quad (13)$$

which has also been applied in topological classification in nanowire systems and quantum systems with geometric driving.⁹⁷⁻¹⁰⁰ It should be reminded here that the wave function for $\lambda < 0$ regime is defined in momentum space as mentioned in Sect. II, thus we should also take spin texture in momentum space where the spin winding is in $\langle\sigma_y\rangle$ - $\langle\sigma_x\rangle$ plane.

Here by Equation (13) a problem arises from the boundary condition as there is a fractional winding angle at infinity. Nevertheless, we can neglect this boundary angle and simply take the nearest integer of n_{zx} as a final effective winding number

$$n_w = \text{nint}(n_{zx}), \quad (14)$$

where the rounding function $\text{nint}(x)$ gives the integer closest to x . This is equivalent to approximately regarding the spin winding in $\langle\sigma_z\rangle$ - $\langle\sigma_x\rangle$ plane as connected at the two ends of $x \rightarrow \pm\infty$ as if periodic condition. In this way, the effective spin winding number n_w is equal to the wave-function node number n_Z in the topological phases of the ground state.

D. Spin Winding Directions

Besides the rounds of the spin winding, the winding direction turns out to be another important feature. The

examples shown in Figure 6 are illustrated in $0 < \lambda < 1$ regime, where the effective winding direction for the low-lying states with a finite number of nodes is more probably counterclockwise like the direction of the polar angle, as indicated by the arrows along the spin trajectories in Figure 6e,f. The effective winding direction can also be clockwise, which happens more probably in $\lambda > 1$ regime as the effective Rashba field g_y changes the sign beyond $\lambda = 1$. We show some examples in **Figure 7** both for the ground state and for excited states. Here, besides the similar correspondence of nodes and spin winding in clockwise direction. Now we realize that the clockwise/counterclockwise winding direction is also a quantum feature that should be emphasized in topological identifications of quantum states in light-matter interactions. Of course, the winding direction can be reflected in the sign of n_w if one does not take the winding number only by its amplitude.

E. A Full Topological Classification for Ground State

Inspired by the above analysis on the nodes and the spin windings, we can combine the parity, the node number and effective winding number to identify different quantum states of the ground state. We present the ground-state phase diagram with a full topological identification in **Figure 8**. Here the numbers represent the node number n_Z , which is equal to the absolute effective spin-winding number n_w for the ground state, the overline (underline) denotes positive (negative) parity, while the positive (negative) sign before the numbers denotes counterclockwise (clockwise) spin winding direction. One can recognize the counterclockwise (clockwise) spin windings in $\lambda < 1$ ($\lambda > 1$) regime. The special unconventional TT mentioned in Sect IV B occurs at the $0/(-1)$ boundary where there is neither gap closing nor parity reversal, in contrast to the other boundaries which are conventional ones.

VI. BIG (BRIDGE) SPIN KNOTS FOR NOVEL TOPOLOGICAL TRANSITIONS

A. Anti-Winding Nodes from Big (Bridge) Spin Knots in Excited States

In last section we have seen the correspondence not only of the wave-function nodes and the spin-winding zeros but also of the node number n_Z and the spin winding number n_w in the ground state. In excited states, the nodes-zeros correspondence from the wave functions and the spin windings always holds but the n_Z - n_w correspondence may be broken, which unveils a different kinds of TTs. Indeed, besides the spin winding around the origin, the spin trajectory can also form spin knots that are not

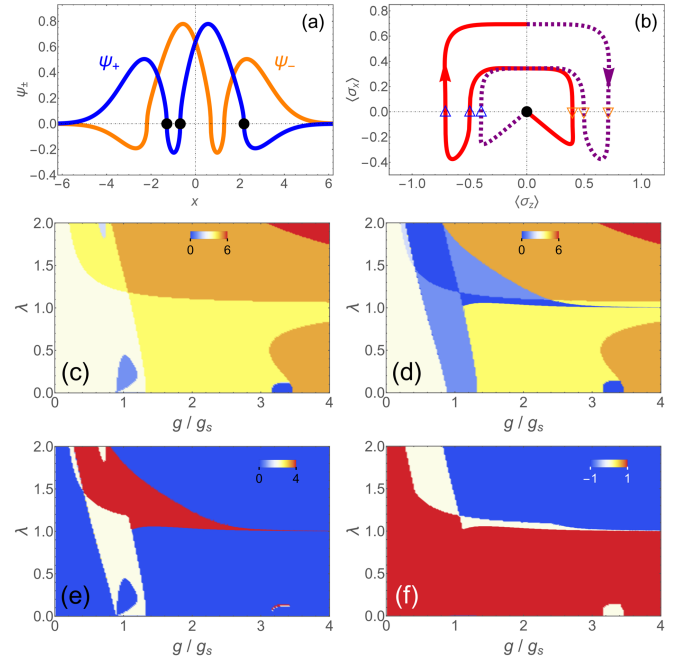


FIG. 9. *Anti-winding-node transitions in excited states.* a,b) Nodes (dots) of the wave function (a) and zeros (triangles) of spin winding in $\langle \sigma_z \rangle$ - $\langle \sigma_x \rangle$ plane (b) at $\lambda = 0.8, g = 0.9g_s$. c-f) Phase diagrams of n_Z (c), $|n_w|$ (d), $n_Z - |n_w|$ (e) and $\text{sign}(n_w)$ (f) in g - λ plane. Here $j_E = 5$ and the plot amplitude is amplified by $|\psi_{\pm}(x)|^{1/2}$ and $\langle \sigma_{x,z}(x) \rangle^{1/3}$ in (a,b).

surrounding the origin. Note such spin knots have no contribution to the spin winding number as the spin trajectory in a spin knot comes back to a same point which cancels the winding angle. When the spin knot is small and not crossing the $\langle \sigma_z \rangle$ axis, as the case in Figure 7f where actually there is a small knot below the origin, the winding number is not affected and n_Z is equal to n_w . However, the spin knot can be also large so that the spin trajectory can cross the $\langle \sigma_z \rangle$ axis to form spin-winding zeros, as in **Figure 9b** where the knot forms a bridge-like profile with two piers crossing the $\langle \sigma_z \rangle$ axis. In this situation the final spin winding number is smaller than the wave-function node number as in Figure 9a. We can name such a knot by *big spin knot* or *bridge spin knot* and the involved nodes by *anti-winding nodes* which do not contribute to the spin windings.

B. Anti-Winding-Node Topological Transitions

When a bridge knot with anti-winding nodes is formed, a new topological transition occurs concerning the difference of the wave-function node number and the spin winding number. Figure 9c shows the phase diagram of n_Z for $j_E = 5$ at $\omega = 0.5\Omega$, with the anisotropy strength extended to $\lambda = 2$. Here the vertically tilting line around $g = 1.0 \sim 1.3g_s$ is the first level crossing line in Figure 4. The corresponding map of n_w is presented in Figure 9d

in which three new main boundaries appear: (i) around $g = 0.3 \sim 0.9g_s$, vertically parallel to the first level crossing line; (ii) horizontally around $\lambda \sim 1$; (iii) the left slash line in $\lambda > 1$ and $g \gtrsim 1.0g_s$ regime. Note the node number n_Z remains unchanged across all these three boundaries while the winding number n_w has a jump, which indicates a new type of TTs. The transition at boundary (i) should be connected with the level anticrossing as the boundary is around the level anticrossing in Figure 4d, thus the level anticrossing is associated not only with node topological transitions but also with anti-winding-node TTs. The transition at boundary (ii) should originate from the sign reversal of g_y around $\lambda = 1$ which changes the relation of the Rashba spin-orbit term and tunneling energy from counteracting to competing.¹⁹ The transition at boundary (iii) may come from a larger g_y that renders the Rashba spin-orbit coupling to dominate over the tunneling.

The discount of winding number n_w by the *anti-winding* spin knots can be seen in Figure 9e which shows

$$n_{aw} = n_Z - |n_w|, \quad (15)$$

denoting the pair number of nodes involved in bridge spin knots. In the blue region n_Z and $|n_w|$ are equal and there is no bridge spin knot, while there is a discount of $|n_Z|$ in other regions where bridge spin knots appear.

The total winding direction is indicated by the sign of n_w in Figure 9f. We see here that the spin is winding counterclockwise in most $\lambda < 1$ regime and also in $\lambda > 1$ regime with small g , while clockwise spin winding is found for large g in $\lambda > 1$ regime. In the white regions, the spin effectively does not wind around the origin.

C. Topological Multiple Points in Excited States

At this point it may be worthwhile to mention the topological multiple points where different topological boundaries meet. The ground state of the anisotropic QRM has a multicritical point and series of quadruple points along $\lambda = 0$ line which however are not topological multiple points but crossings of transitions in topological class and Landau class.^{19,20} While there is a symmetry breaking in traditional transitions of Landau class, TTs preserve the symmetry. Indeed, as one sees in Figure 8, the topological boundaries do not cross each other in the ground state, although the presence of the nonlinear Stark coupling can create topological quadruple points.²¹ Here from Figures 4c,5c,9c-e we see that the topological multiple points can occur in the excited states without introducing the Stark coupling. These topological multiple points have various crossings among unconventional TT boundaries, conventional ones, and anti-winding-node ones. The regimes around the topological multiple points are topologically sensitive to the parameter variations which might be useful to design topological

quantum devices or sensors, while different types of multiple points could provide more varieties or choices in need.

VII. NODE SORTING AND ALGEBRAIC FORMULATION FOR GENERAL SPIN WINDING NUMBER WITH SPIN KNOTS

A. Another Set of Wave-Function Nodes on Spin- σ_x Basis

So far we have only considered the nodes in the wave function component $\psi_{\pm}(x)$ on spin- σ_z basis $|\uparrow\rangle, |\downarrow\rangle$. We can also transform to spin- σ_x basis $|\uparrow\rangle = (|\uparrow\rangle + |\downarrow\rangle)/\sqrt{2}$, $|\downarrow\rangle = (|\uparrow\rangle - |\downarrow\rangle)/\sqrt{2}$ by $|\psi(x)\rangle = \psi_+(x)|\uparrow\rangle + \psi_-(x)|\downarrow\rangle = \tilde{\psi}_+(x)|\uparrow\rangle + \tilde{\psi}_-(x)|\downarrow\rangle$ where

$$\tilde{\psi}_{\pm}(x) = \frac{1}{\sqrt{2}} [\psi_+(x) \pm \psi_-(x)]. \quad (16)$$

Note $\tilde{\psi}_{\pm}(x)$ can also have nodes $x = y_{Z,j}$ which actually correspond to the zeros of $\langle\sigma_z(x)\rangle$

$$\tilde{\psi}_+(y_{Z,j}) \text{ or } \tilde{\psi}_-(y_{Z,j}) = 0, \quad \langle\sigma_z(y_{Z,j})\rangle = 0, \quad (17)$$

at equal wave-function amplitudes of $\psi_{\pm}(x)$,

$$|\psi_+(y_{Z,j})| = |\psi_-(y_{Z,j})|, \quad (18)$$

as concluded from Equations (5) and (8). Note here under the parity symmetry the two wave-function components $\tilde{\psi}_{\pm}(x) = \frac{1}{\sqrt{2}} [\psi_+(x) \pm P\psi_+(-x)]$ have different space inversion symmetries (symmetric and anti-symmetric), thus having different node situations. It is more convenient to take (18) for locations of $y_{Z,j}$. As addressed below we find the topological information of the spin windings and spin knots is encoded in the order of the $\psi_{\pm}(x)$ nodes $x_{Z,i}$ and the $\tilde{\psi}_{\pm}(x)$ nodes $y_{Z,j}$, where i, j are number labeling for multi-node case.

B. Node Sorting and Algebraic Formulation of Spin Winding Number

Since the spin winding will finally go through these nodes or zeros, we propose an alternative way to calculate the winding number in terms of the node numbers of $\psi_{\pm}(x)$ and $\tilde{\psi}_{\pm}(x)$ or equivalently the zero numbers of $\langle\sigma_x(x)\rangle$ and $\langle\sigma_z(x)\rangle$.

Suppose $x_{Z,1} < x_{Z,2} \cdots < x_{Z,2n_Z}$ are the nodes of $\psi_{\pm}(x)$ or equivalently the zeros of $\langle\sigma_x(x)\rangle$, then we introduce $n_Z^{(+,-)}$ to count the nodes among the original ones $\{x_{Z,k} | k = 1, \dots, 2n_Z\}$ that change the sign of $\langle\sigma_z(x_{Z,k})\rangle$, i.e. $x_{Z,1} = x_{Z,1}^{(+,-)} < x_{Z,2}^{(+,-)} \cdots < x_{Z,2n_Z}^{(+,-)}$ at which $\langle\sigma_z(x_{Z,i}^{(+,-)})\rangle \times \langle\sigma_z(x_{Z,i+1}^{(+,-)})\rangle < 0$. We denote the sign of $\langle\sigma_z(x_{Z,i}^{(+,-)})\rangle$ by $S_i^{(+,-)}$.

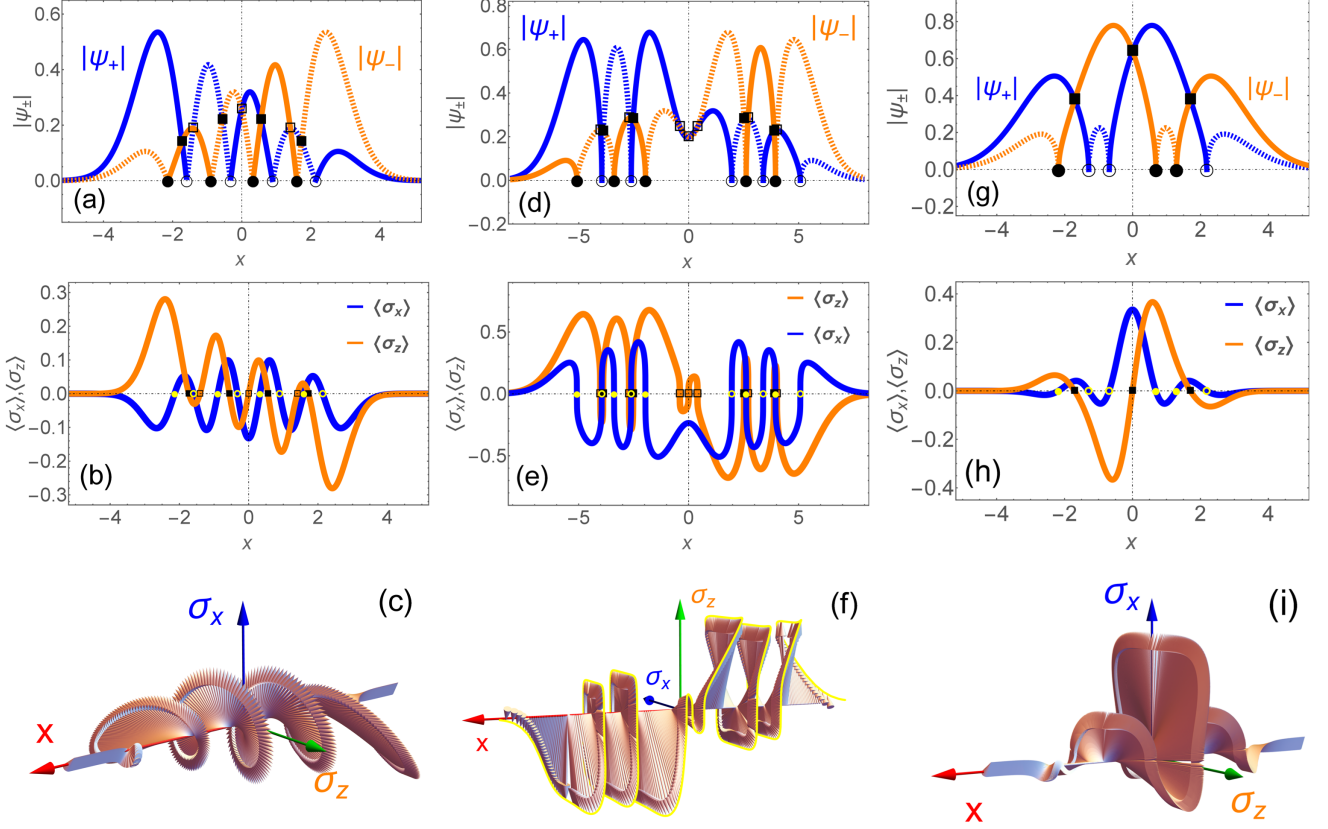


FIG. 10. *Node distribution order and algebraic formulation for general spin windings.* Wave-function amplitudes $|\psi_+(x)|$ (blue) and $|\psi_-(x)|$ (orange) (a,d,g), instantaneous spin expectations $\langle\sigma_x(x)\rangle$ (blue) and $\langle\sigma_z(x)\rangle$ (orange) (b,e,h), three-dimensional spin texture (c,f,i) for $j_E = 5$ at: a-c) $\lambda = 0.2$ and $g = 1.5g_s$ without spin knot, corresponding to Figure 6f; d-f) $\lambda = 3.0$ and $g = 1.7g_s$ with a small knot, corresponding to Figure 7f; g-i) $\lambda = 0.8$ and $g = 0.9g_s$ with a big knot and anti-winding nodes, corresponding to Figure 9b. In (a,d,g) solid (dotted) lines represent $\psi_{\pm}(x) = |\psi_{\pm}(x)|$ ($\psi_{\pm}(x) = -|\psi_{\pm}(x)|$). In (a,d,g) circles (squares) are nodes of $\psi_{\pm}(x)$ ($\tilde{\psi}_{\pm}$), correspondingly in (b,e,h) filled (empty) circles mark $\langle\sigma_x(x)\rangle$ zeros with positive (negative) $\langle\sigma_z(x)\rangle$, while filled (empty) squares denote $\langle\sigma_z(x)\rangle$ zeros with positive (negative) $\langle\sigma_x(x)\rangle$.

Let $m(i)$ count the nodes $y_{Z,j}$ ($j = 1, \dots, m(i)$) of $\langle\sigma_z(x)\rangle$ (not $\langle\sigma_x(x)\rangle$) in the section $[x_{Z,i}^{(+,-)}, x_{Z,i+1}^{(+,-)}]$ and each node $y_{Z,j}$ acquires a negative (positive) sign denoted by s_j^i for negative (positive) $\langle\sigma_x(y_{Z,j})\rangle$. Generally $m(i)$ is an odd number in an effective contribution to the final winding number, since an even $m(i)$ means the spin trajectory is returning thus cancels the winding angle.

With the above node sorting we obtain an algebraic formula for the spin winding number

$$n_w = n_w^Z \equiv \sum_{i=1}^{n_Z^{(+,-)}} n_{w,i}^Z, \quad (19)$$

$$n_{w,i}^Z = \frac{1}{4} \left[1 - (-1)^{m(i)} \right] S_i^{(+,-)} s_{m(i)}^i, \quad (20)$$

as a replacement of the integral form of spin winding number in Equations (13) and (14). Here, as mentioned in Section VC, we regard the spin winding as connected at the two infinity ends $x \rightarrow \pm\infty$ in $\langle\sigma_z\rangle$ - $\langle\sigma_x\rangle$ plane, thus the $n_Z^{(+,-)}$ 'th section is composed of $[x_{Z,n_Z^{(+,-)}}^{(+,-)}, \infty)$

and $(-\infty, x_{Z,1}]$. Then the two infinity ends together contribute once to $m(n_Z^{(+,-)})$ with the sign equal to that of $\langle\sigma_x(x)\rangle|_{x \rightarrow \infty}$. Of course, in principle $m(n_Z^{(+,-)})$ can also be larger than 1, since in the $n_Z^{(+,-)}$ 'th section there could be $\langle\sigma_z(x)\rangle$ zeros besides the contribution of the connected infinity boundary.

C. Illustrations of Node Sorting in the Absence/Presence of Spin Knots

To see more clearly the relation of spin winding number and the node sorting, in Figure 10 we illustrate some typical examples of wave-function amplitudes $|\psi_{\pm}(x)|$ and spin textures, without spin knots (a-c), with a small knot (d-f), and with a big (bridge) knot with anti-winding nodes (g-i), respectively corresponding to Figures 6f, 7f, and 9b.

In Figure 10a,d,g the nodes of $\psi_{\pm}(x)$ are marked by black filled (empty) circles which correspond to the ze-

ros of $\langle\sigma_x(x)\rangle$ while $\langle\sigma_z(x)\rangle$ is positive (negative), as determined by the relations $\langle\sigma_x(x)\rangle = 2\psi_+(x)\psi_-(x)$ and $\langle\sigma_z(x)\rangle = |\psi_+(x)|^2 - |\psi_-(x)|^2$. We see that all $\psi_+(x)$ nodes (empty circles) have negative $\langle\sigma_z(x)\rangle$ while all $\psi_-(x)$ nodes (filled circles) have positive $\langle\sigma_z(x)\rangle$. On the other hand, the nodes of $\tilde{\psi}_\pm(x)$ or the zeros of $\langle\sigma_z(x)\rangle$ are located at points where $|\psi_+(x)|$ and $|\psi_-(x)|$ are equal, either with same signs (filled squares) of $\psi_+(x)$ and $\psi_-(x)$ at crossings of both solid lines or both dotted lines or with opposite signs (empty squares) of $\psi_+(x)$ and $\psi_-(x)$ at crossings of solid lines and dotted lines, the former yields positive $\langle\sigma_x(x)\rangle$ while the latter gives negative $\langle\sigma_x(x)\rangle$. The filled/empty circles and squares in Figure 10b,e,h represent the zeros and signs of $\langle\sigma_x(x)\rangle$ and $\langle\sigma_z(x)\rangle$ the same as in Figure 10a,d,g.

Figure 10a,b show a completely alternate node or zero sequence, filled-circle/filled-square/empty-circle/empty-square/filled-circle/..., indicating full spin windings without any spin knot as in two-dimensional Figure 6f and three-dimensional Figure 10c. Figure 10d-f include a small spin knot (in $\langle\sigma_z(x)\rangle$ - $\langle\sigma_x(x)\rangle$ plane in Figure 7f) around $x = 0$ as displayed by the successive empty squares (zeros of $\langle\sigma_z(x)\rangle$) during the turns of spin trajectory. Nevertheless, the successive squares appear between a same pair of filled and empty circles, thus not affecting the equality of the winding number n_w and the node number n_Z . However, the successive filled squares in Figure 6g,h show up in different pairs of filled and empty circles, which invalidates the node number in contribution to the winding number. Finally the two cases in Figure 10a-f have $|n_w| = |n_w^Z| = n_Z$ while the case in Figure 10g-i has $|n_w| = |n_w^Z| < |n_Z|$.

D. Topological Identity and Bridge of Geometric Topology and Algebraic Topology

One may find the convenience of Equation (19) that by replacement of n_w with n_w^Z it numerically avoids the more difficult integral in the original winding expression (13) for n_w which involves derivatives. More importantly it demonstrates the relation of wave-function nodes and spin windings in an explicit and solid way. The integral in n_w depends on the topological structure of spin trajectory geometrically, while the nodes and the sorting involved in n_w^Z reflect the topological information of the wave function or the spin texture algebraically. The equation also reclaims the original sense of topological classification that no matter how the spin trajectory is geometrically deformed one has the same topological winding number as long as the few points of node sequence are given, just as one cannot change a torus into a sphere by a continuous deformation in the well-known illustration for topological difference where the holes of an object are given.

Besides the algebraic nature of the nodes themselves as in a function, one can also relabel the nodes with four numbers so that the node topological information

is more clearly represented by the a sequence code of the four numbers. Different sorting and ordering of the numbers give different topology, which is a kind of algebraic topology. For an example, we can assign the numbers as these following the symbols: filled circle (1), filled square (2), empty circle (3) and empty square (4). Then the node number code for a smooth counterclockwise winding as in Figure 10a-c is 1234123412341234, while exchange of 2 and 4 gives a clockwise winding $\dots 14321432\dots$. Here, the digit with tilde is coming from the two infinity ends which are assumed to be connected in Section VII B and $\tilde{2}$ ($\tilde{4}$) stands for same (opposite) sign of $\psi_+(x)$ and $\psi_-(x)$ or equivalently positive (negative) value of $\langle\sigma_x(x)\rangle$ at $x \rightarrow \pm\infty$. Each period means a round of winding. A section with adjacently repeating 2 or 4 denotes a small knot as in Figure 10d-f which have a clockwise code 1432143214443214321432 with three adjacent 4s in the middle. An anti-winding big spin knot will break the code order either 1234 or 1432, as in Figure 10g-i which are embedded a disordered code 1233211234. Such a node code provides a topological identity to label the topological structure of the eigenstate.

In such a sense, Equation (19) also builds the bridge of geometric topology and algebraic topology, but in a physical way as the nodes are originally of the wave function and the windings are of the spin in a quantum mechanical system. The mapping of topological structure of the quantum states onto number sequences may provide a way for topological quantum encoding and decoding.

VIII. HIDDEN TRANSITIONS OF SPIN KNOTS

The topology of knot depends on what criterion one adopts. For a rope in three-dimensional space, a knot with only one returning loop can be continuously deformed into a straight line, such a knot topologically is equal to a straight line. However in a two-dimensional plane, if one counts the number of holes formed by loops of returning paths and classify the topology by the corresponding fixed hole numbers, a knot is then topologically different from a straight line. In this sense, spin knots reflect a different level of topological information apart from the topology of wave-function nodes on an axis and spin winding around the origin. In this section we shall explore more hidden transitions induced by spin knots.

A. Small (Scallop) Knot Transitions in Ground State

As mentioned in Section VI, *small spin knots* are formed around $\langle\sigma_x(x)\rangle$. We term small knot not by its absolute size but by the characteristic that it only covers either positive or negative $\langle\sigma_x(x)\rangle$ axis but not across the $\langle\sigma_z(x)\rangle$ axis as the big (bridge) knots. Small spin knots do not break the correspondence of wave-function node numbers and the spin winding numbers, but they

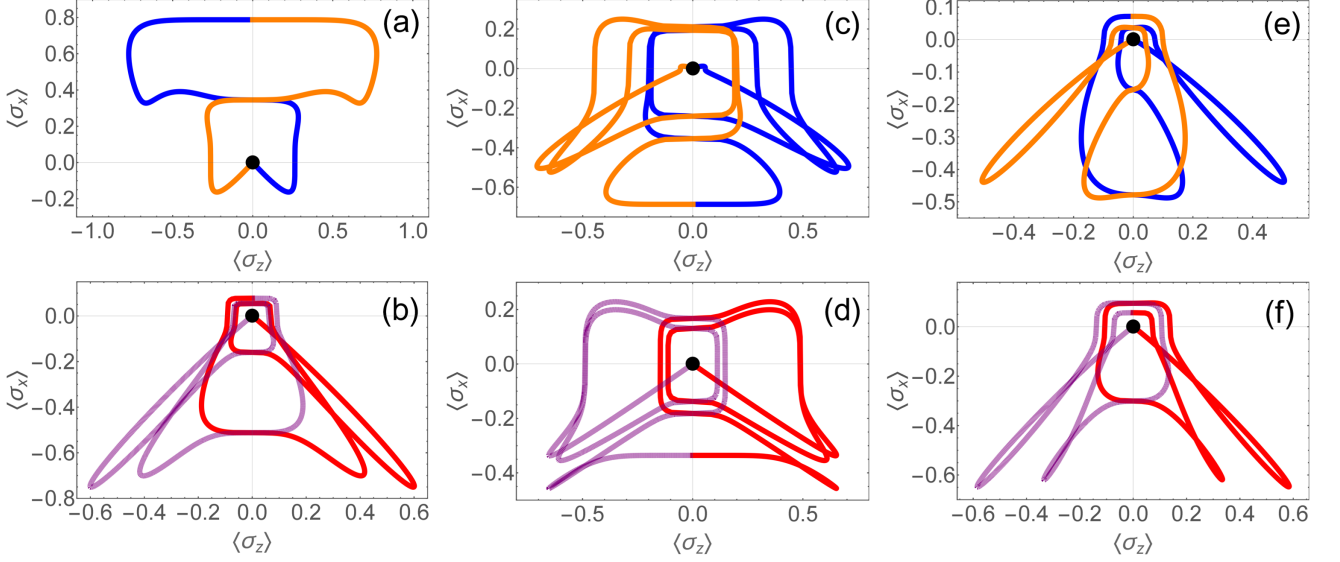


FIG. 11. Typical spin windings with different kinds of knots in excited states: Anisotropic QRM as a born topological abstract artist. Spin windings in formal or spiritual similarity with a) a chef in a biggest hat, and with beard ($g = 1.0g_s, \lambda = 0.2$); b) a sumo wrestler ($g = 0.1g_s, \lambda = 3.0$); c) a little girl with twin ponytails ($g = 1.2g_s, \lambda = 1.5$); d) a lady with luxuriant hair and shawl ($g = 3.4g_s, \lambda = 0.8$); e) an emperor penguin ($g = 0.4g_s, \lambda = 2.0$); f) an outward-flying swallow in radar-invading mode ($g = 0.22g_s, \lambda = 2.0$). For a better visibility the spin amplitude is amplified by $\langle \sigma_{z,x} \rangle^A$ with $A = 1/4, 1/2, 1/3$ for (a-d), (e), (f) respectively. Here $j_E = 5$ and $\{n_Z, n_w, n_{ex}, n_{DK}\} = \{1, 1, 2, 0\}$ (a), $\{3, -3, 2, 0\}$ (b), $\{5, -1, 2, 0\}$ (c), $\{4, 4, 2, 2\}$ (d), $\{4, 0, 4, 2\}$ (e), $\{3, 3, 0, 4\}$ (f).

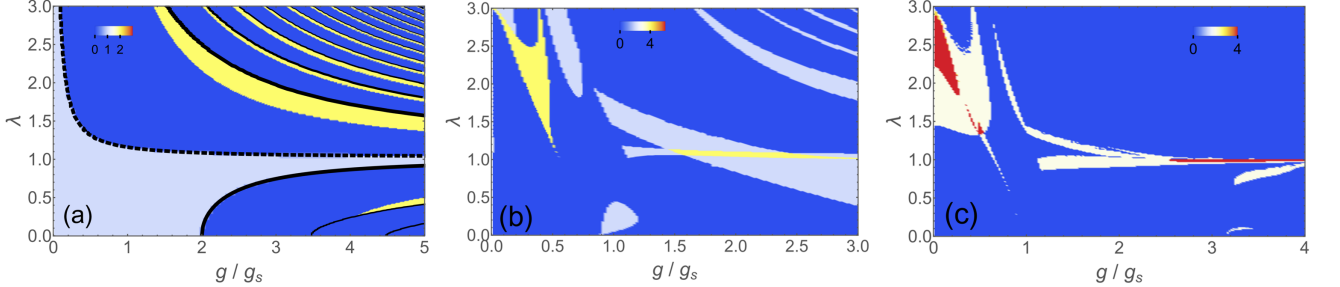


FIG. 12. a) Phase diagram of n_{ex} in the ground state: Hidden small-spin-knot transitions. The solid and dashed lines mark the previous conventional and unconventional TTs for comparison. b) Phase diagram of n_{ex} for state $j_E = 5$. c) Phase diagram of n_{DK} for excited state $j_E = 5$.

change the number of $\langle \sigma_z(x) \rangle$ zeros. We show a small knot in **Figure 11a**, where although the knot appears like a biggest hat of chef the knot does not span or bend to cross the $\langle \sigma_z(x) \rangle$ axis. The knot profile in **Figure 11a** also reminds us of the exotic shark scalloped hammer-head, while the small knot can also be really small as a pearl in a scallop (e.g. in **Figure 7f**). The feature of scallop shape here most distinguished from the big bridge knot is that scallop never has bridge piers. So we also call a small knot *scallop knot* if terming a group of knots by size is not a good way.

At this point it should be mentioned that the small (scallop) knot can also be formed by the two infinity ends which are regarded as connected, as mentioned in **Section VII B**, which can be tracked down by the condition $|m(n_Z^{(+,-)})| > 1$. We show an example in **Figure 11b**

which looks like a sumo wrestler. As one may recognizes the two arms are starting from the origin dot, which corresponds to infinity in x space, and form a small knot at the neck position.

The node sorting and algebraic formulation for spin windings in last section inspires a way to monitor the small spin knots quantitatively. We propose the following quantity

$$n_{ex} = \sum_{i=1}^{n_Z^{(+,-)}} (m(i) - 1), \quad (21)$$

which actually denotes the *extra* zero number of $\langle \sigma_z(x) \rangle$ on $\langle \sigma_x(x) \rangle$ axis formed by the returning of the spin trajectory apart from the first time going across the $\langle \sigma_x(x) \rangle$ axis. Note that not only the knotless winding is not in-

cluded in n_{ex} but also the bridge knot is excluded, thus n_{ex} can make a distinction from these cases and extract a deeper topological information apart from n_Z and n_{aw} . A vanishing n_{ex} guarantees no small knots, while $n_{ex} = 2$ means the existence of a small spin knot. An odd number of n_{ex} indicates both vanishing n_Z and n_w , e.g. as in Figure 9c where the blue island around $g = 3.3g_s, \lambda = 0.1$ where $n_{ex} = 3$. Although $n_{ex} = 1$ corresponds to the topologically trivial case as in Figure 6a a larger odd number will mean spin knots despite of no effective winding.

Indeed, although there are no anti-winding large knots in the ground state, small-knot transition can still occur. We show n_{ex} of the ground state in Figure 12a. As one sees n_{ex} is zero (blue) in most regions while, apart from $n_{ex} = 1$ in the no-node region (light blue), another finite value ($n_{ex} = 2$) appears in slim yellow belts adjacent to the conventional topological boundaries with level closing (black solid lines). These belt regions show the presence of a small spin knot, which occurs mostly in $\lambda > 1$ regime and turns to be thin silvers in regime of larger λ and g . It should be mentioned here that, unlike the chef hat in Figure 11a, the spin knot in the ground state is really small as in Figure 7f. These new transitions emerge in gapped situation, thus also being unconventional TTs in addition to the previous unconventional boundary (black dashed line) found from transition of the wave-function nodes in the gapped phase.

To sum up, now for the ground state we have two kinds of unconventional TTs in different levels, one from the node transition, the other from the small-spin-knot transition.

B. Huge (Hug) Knots in Excited States

The formulation of n_{ex} in (21) helps us to reveal knots beyond the small and big ones. In fact, apart from the odd-number case which has no effective winding as mentioned below Equation (21), an even number of n_{ex} larger than 2 is also possible and can occur in three cases: (i) there are more than one small knots but each appears in different position section $[x_{Z,i}^{(+,-)}, x_{Z,i+1}^{(+,-)}]$; (ii) more than one small knots within a same section $[x_{Z,i}^{(+,-)}, x_{Z,i+1}^{(+,-)}]$, (iii) there are some *huge knots* that span over positive and negative $\langle \sigma_x(x) \rangle$ axes through $\langle \sigma_z(x) \rangle$ axis. Case (i) belongs to the afore-mentioned normal small knots. Case (ii) is rare in low-lying states. Case (iii) is more often. We give an example of case (iii) in Figure 11e where the spin trajectory draws a shape of penguin. One sees that two huge knots are hugging the origin to build the head, body and leg parts of the penguin. With this hugging shape we also call the huge knots *hug knots*.

C. Diagonal (Dipterus) Knots in Excited States

The huge (Hug) knots revealed by n_{ex} again leads to our finding of another kind of knots which are distinguished from all the afore-addressed small, big and huge knots. In the penguin-like case we also see the two fins of the penguin which form two narrow spin knots. These knots are not located on the $\langle \sigma_x(x) \rangle$ or $\langle \sigma_z(x) \rangle$ axis as the small, big and huge knots but have orientations between the axes, which we call *diagonal Knots*. Note that, except the condition of being away from the axes where the spin zeros are located, the diagonal knots are not directly associated with the zeros of $\langle \sigma_x(x) \rangle$ or $\langle \sigma_z(x) \rangle$. Nevertheless, they can be tracked down by the equal-spin condition

$$\langle \sigma_z(x_1) \rangle + i \langle \sigma_x(x_1) \rangle = \langle \sigma_z(x_2) \rangle + i \langle \sigma_x(x_2) \rangle, \quad (22)$$

of two different points x_1, x_2 between a $\langle \sigma_x(x) \rangle$ zero and a neighboring $\langle \sigma_z(x) \rangle$ zero. We can also have more pairs of diagonal knots in a same state, as in Figure 11f where the spin winding draws a shape like an outward-flying swallow. As in radar-invading mode we don't see much of the wide wings which appear to be two narrow diagonal knots. However, the body and tail of the swallow are not in a good stealth and we see the forked tail that appears to be another two diagonal knots. Considering the above penguin and swallow examples, we also call diagonal knots *dipterus knots*.

D. Composite Knots in Excited States

We have introduced different kinds of knots in different states. One can also have different kinds of knots in a same excited state. For an example, Figure 11c shows a spin winding with a little-girl-alike shape. The twin ponytails from the top are two big knots, while the shoulder is a small knot around negative- $\langle \sigma_x(x) \rangle$ axis. These two kinds of knots appear in a same state but well separated in the evolution with respect to x . The state in Figure 11e with a penguin shape has two huge knots and two diagonal knots at the same time. Although the huge knots have an overwhelming size, basically the huge knots and the diagonal knots are not mixing up with each other. Still, there can be composite knots by mixed knots. We show a case in Figure 11d which abstractly looks like a lady with luxuriant hair. Note the hair style is changed from twin ponytails in Figure 11c to thick layered Bob, there are no anti-winding-node large knots now. Of course one can also have braids formed by diagonal knots if moving a bit to around $\lambda = 1$, we don't show the figures lest some one should think we are opening a hair salon. Here in Figure 11d the shoulder changes to be a shawl-like shape which actually is composed of one small knot around negative- $\langle \sigma_x(x) \rangle$ axis and two diagonal knots. Note the diagonal knots are formed within the small knot, thus turning out to be a composite knot. If

we look back at Figure 11c with the little-girl shape, the left ponytail, the shoulder and the right ponytail together actually form a giant composite knot which meanders in a complicated returning path with canceling in winding and several times of switching back and braiding.

E. A Full Topological Identity Encoding Including Diagonal Spin Knots

Since the newly found diagonal knots are not directly associated with the nodes of wave function or equivalently the zeros of the spin winding, we can assign a distinguished number, e.g. 5, to a diagonal knot in the topological code of eigenstate as mentioned in Section VII D. Thus, the topological code now includes three angles or levels of topological information: (i) the digits 1,3 represent the nodes of $\psi_{\pm}(x)$, i.e., the $\langle\sigma_x(x)\rangle$ zeros on positive-,negative- $\langle\sigma_z(x)\rangle$ axes in $\langle\sigma_z(x)\rangle$ - $\langle\sigma_x(x)\rangle$ plane; (ii) the digits 2,4 denote the nodes of $\psi_{\pm}(x)$, i.e, the $\langle\sigma_z(x)\rangle$ zeros on positive-,negative- $\langle\sigma_x(x)\rangle$ axes; (iii) the digit 5 marks a diagonal spin knot. For an example, Figure 11e has two diagonal knots on the infinity sides which contribute two 5s in the two ends of the corresponding topological code 5123443214412354. The digital order of the code reflects the detailed topological structure. Then, such a code encodes a full topological information of the eigenstate.

F. Phase Diagrams of Extra Zeros and Diagonal Knots

Besides the small-knot phase diagram of the ground state in Figure 12a, for the excited states we show the phase diagrams of the extra zero number n_{ex} on $\langle\sigma_x(x)\rangle$ axis and diagonal-knot number n_{DK} in Figure 12b,c. We see that small knots not only appear in large- g , λ regime similarly to the ground state, but also emerge in intermediate- and small- λ regimes for a coupling $g \gtrsim g_s$. Huge knots are formed in the large- λ but small- g regime. Diagonal knots show up not only in large- λ and small- g regime also also possible around $\lambda = 1$ for $g \gtrsim g_s$. Simultaneous appearances of different kinds of knots can be found in the overlapping regime of these phase diagrams as well as those in Figure 9e.

G. Anisotropic QRM as a Born Abstract Artist

As in the above descriptions for different knots we are surprised to find that the sophisticated drawings of the spin windings in Figure 11a-f really have amazing spiritual similarity with a chef in a biggest hat and with beard, a sumo wrestler, a little girl with twin ponytails, a lady with luxuriant hair and shawl, an emperor penguin, and an outward-flying swallow in radar-invading mode, respectively. One may wonder about Figure 9b to

which we have not paid attention before as a painting but now we see a beard judge in wigs or one may say a pilot in helmet and oxygen mask. It should be mentioned that, except for the finite numbers of n_{ex} , n_{DK} in Figure 12b,c, these figure illustrations are chosen not deliberately, as one can see from the corresponding parameter digits which are not fine-tuned. In fact, we simply pick up a point in the n_{ex} , n_{DK} phase diagrams quite randomly and it just turns out to be an artistic work. One may question about the earlier works in Figures 6,7 which were not in the art gallery. Well ... what we can interpret first is: Figure 7f may be some star gate or teleportation device and Figure 6e is the corresponding exit tunnel. We are not sure whether or not the teleportation is done with full fidelity for which one has to pray before going out of the exit. For the other panels one needs to put upside down: In Figure 7 panel (a) is a butterfly spy (probably still in experimental stage), panel (p) is a devilbat associated from devilfish or a Carnival cat mask; In Figure 9 panel (j) is a lotus flower, and finally panel (p) is without doubt the most abstract portrait in the world of an extraterrestrial being who even seems to be quite amiable.

Amazed by the painting sophistication, abstraction, imagination, spirituality, quality, variety, prolificity, and so forth, we cannot help drawing the conclusion that the anisotropic QRM is a born topological abstract artist¹⁰⁶ whose talent apparently has been buried in the numerous findings about the QRM and its extensions including symmetry,⁵⁴⁻⁵⁷ various patterns of symmetry breaking,^{18,19,22} few-body QPTs,^{4,13-22} multicriticalities and multiple points,¹⁸⁻²¹ universality classification,^{11,15,16,19,21} spectral collapse,^{29-31,41,44} photon blockade effect,^{36,37} spectral conical intersections,³⁸ classical-quantum correspondence,¹² single-qubit topological phase transitions,¹⁹⁻²¹ and so on. Since the anisotropic QRM might be the Picasso¹⁰⁷ of physical models, maybe now it is the moment to give some voice to art.

IX. CONCLUSIONS AND DISCUSSIONS

With the exploration of underlying TTs via a thorough study on wave-function nodes and spin windings, we have shed a new light on the energy spectrum of the anisotropic QRM which is the fundamental model of light-matter interactions with indispensable counter-rotating terms in ultra-strong couplings.

On the one hand, by tracking the variation of node numbers in the eigen wave functions, besides the conventional TTs at level crossings we have revealed emerging unconventional TTs without gap closing or parity reversal underlying the level anticrossings. Such level-anticrossing-connected unconventional TTs do not occur in the ground state due to the absence of level anti-crossing, which accounts for the pureness of the ground

state topological phase diagram. Apart from the level-anticrossing-connected unconventional TTs, a particular unconventional TT without level anticrossing is also found and turns out to be universal for the ground state and excited states. This particular transition have several advantages in potential applications for quantum sensors or devices, such as large gap situation, without limitation to ground state, and being applicable for all coupling regimes.

On the other hand, we find that the wave-function nodes have a correspondence to the zeros of spin windings, which endows the nodes a more explicit topological character and provides a physical support for single-qubit topological phase transitions. Thus, the node number or spin winding number can be used as quantum topological numbers along with the parity to characterize the quantum states especially in the ground states. In such a topological classification, the clockwise/counterclockwise direction of the spin winding adds another quantum feature to further distinguish the various quantum states of light-matter interactions.

Moreover, when the wave-function node number is corresponding to the spin winding number in the ground state, another kind of TTs arise in the excited states with unmatched node number and winding number due to the emerging anti-winding spin knots. Hidden transitions of small knots are found for the ground state, while in excited states transitions of different spin knots emerge including small (scallop), big (bridge), huge (hug) and diagonal (dipterus) ones. The analysis on the node sorting and ordering leads us to an algebraic formulation of the spin winding number which originally is in integral form, building a bridge of geometric topology and algebraic topology in a physical way concerning the wave function and the spin windings.

Since the spin is a physical quantity, the topological information originally encoded in the topological structure of the wave function now can be decoded by the spin texture. Such a physical decoding not only turns the

topological information to be detectable, but also might provide possibility for designing topological quantum devices or sensors. In such a perspective, both the conventional TTs and unconventional ones addressed in the present work might have some potential applications as both gap-closing³³ and gapped³⁵ situations are applicable, while the unconventional TTs might have some more advantage in avoiding the detrimental slowing-down effect close to transitions.³⁵

It should be noted that the anisotropic QRM considered in the present work is a realistic model which can be implemented in superconducting circuits with possible access to ultra-strong^{5,61-70} and even deep-strong couplings,^{70,71} while the interaction anisotropy is also highly tunable.^{27,61,89} Experimentally in such circuit systems^{95,108,109} the effective position x (momentum p) can be simulated by the flux (charge) of Josephson junctions which can be continuously tuned and the spin texture might be measured by interference devices and magnetometer.¹⁰⁹ We speculate tests or applications of our results might be feasible in these platforms. On the other hand, our analysis and the gained insight might also be helpful or relevant for some other systems as our model shares some similarity with those in nanowires,⁹⁶⁻¹⁰⁰ cold atoms^{101,105} and relativistic systems.¹¹⁰

As a final remark, our finding shows that the anisotropic QRM might be the Picasso¹⁰⁷ of physical model community. To this extent, one may think art is starting to join the dialogue between mathematics and physics² which was triggered by the milestone work of D. Braak¹ on the integrability of the QRM as mentioned in the beginning of Introduction.

ACKNOWLEDGEMENTS

This work was supported by the National Natural Science Foundation of China (Grant No. 11974151).

-
- [1] D. Braak, *Phys. Rev. Lett.* **2011**, *107*, 100401.
 - [2] E. Solano, *Physics* **2011**, *4*, 68.
 - [3] See a review of theoretical methods for light-matter interactions in A. Le Boité, *Adv. Quantum Technol.* **2020**, *3*, 1900140.
 - [4] See a review of quantum phase transitions in light-matter interactions e.g. in J. Liu, M. Liu, Z.-J. Ying, H.-G. Luo, *Adv. Quantum Technol.* **2021**, *4*, 2000139.
 - [5] P. Forn-Díaz, L. Lamata, E. Rico, J. Kono, E. Solano, *Rev. Mod. Phys.* **2019**, *91*, 025005.
 - [6] A. F. Kockum, A. Miranowicz, S. De Liberato, S. Savasta, F. Nori, *Nature Reviews Physics* **2019**, *1*, 19.
 - [7] F. A. Wolf, M. Kollar, D. Braak, *Phys. Rev. A* **2012**, *85*, 053817.
 - [8] S. Felicetti, A. Le Boité, *Phys. Rev. Lett.* **2020**, *124*, 040404.
 - [9] S. Felicetti, M.-J. Hwang, A. Le Boité, *Phys. Rev. A* **2018**, *98*, 053859.
 - [10] E. K. Irish, J. Gea-Banacloche, *Phys. Rev. B* **2014**, *89*, 085421.
 - [11] J. Larson, E. K. Irish, *J. Phys. A: Math. Theor.* **2017**, *50*, 174002.
 - [12] E. K. Irish, A. D. Armour, arXiv:2203.17147, **2022**.
 - [13] S. Ashhab, *Phys. Rev. A* **2013**, *87*, 013826.
 - [14] Z.-J. Ying, M. Liu, H.-G. Luo, H.-Q. Lin, J. Q. You, *Phys. Rev. A* **2015**, *92*, 053823.
 - [15] M.-J. Hwang, R. Puebla, M. B. Plenio, *Phys. Rev. Lett.* **2015**, *115*, 180404.
 - [16] M. Liu, S. Chesi, Z.-J. Ying, X. Chen, H.-G. Luo, H.-Q. Lin, *Phys. Rev. Lett.* **2017**, *119*, 220601.
 - [17] M.-J. Hwang and M. B. Plenio, *Phys. Rev. Lett.* **2016**, *117*, 123602.
 - [18] Z.-J. Ying, *Phys. Rev. A* **2021**, *103*, 063701.

- [19] Z.-J. Ying, *Adv. Quantum Technol.* **2022**, *5*, 2100088.
- [20] Z.-J. Ying, *Adv. Quantum Technol.* **2022**, *5*, 2100165.
- [21] Z.-J. Ying, *Adv. Quantum Technol.* **2022**, 2200068. (In production)
- [22] Z.-J. Ying, L. Cong, X.-M. Sun, arXiv:1804.08128, **2018**; *J. Phys. A: Math. Theor.* **2020**, *53*, 345301.
- [23] R. Grimaudo, A. S. M. de Castro, A. Messina, E. Solano, D. Valenti, arXiv:2211.07207, **2020**.
- [24] D. Braak, Q.H. Chen, M.T. Batchelor, E. Solano, *J. Phys. A Math. Theor.* **49**, 300301 (2016).
- [25] H. P. Eckle, H. Johannesson, *J. Phys. A: Math. Theor.* **2017**, *50*, 294004.
- [26] Y.-Q. Shi, L. Cong, H.-P. Eckle, *Phys. Rev. A* **2022** *105*, 062450.
- [27] Q.-T. Xie, S. Cui, J.-P. Cao, L. Amico, H. Fan, *Phys. Rev. X* **2014**, *4*, 021046.
- [28] S. Felicetti, D. Z. Rossatto, E. Rico, E. Solano, P. Forn-Díaz, *Phys. Rev. A* **2018**, *97*, 013851.
- [29] S. Felicetti, J. S. Pedernales, I. L. Egusquiza, G. Romero, L. Lamata, D. Braak, E. Solano, *Phys. Rev. A* **2015**, *92*, 033817.
- [30] L. Garbe, I. L. Egusquiza, E. Solano, C. Ciuti, T. Coudreau, P. Milman, S. Felicetti, *Phys. Rev. A* **2017**, *95*, 053854.
- [31] R. J. A. Rico, F. H. Maldonado-Villamizar, B. M. Rodriguez-Lara, *Phys. Rev. A* **2020**, *101*, 063825.
- [32] L. Garbe, M. Bina, A. Keller, M. G.A. Paris, S. Felicetti, *Phys. Rev. Lett.* **2020**, *124*, 120504.
- [33] L. Garbe, O. Abah, S. Felicetti, R. Puebla, *Phys. Rev. Research* **2022**, *4*, 043061
- [34] T. Ilias, D. Yang, S. F. Huelga, M. B. Plenio, *PRX Quantum* **2022**, *3*, 010354.
- [35] Z.-J. Ying, S. Felicetti, G. Liu, D. Braak, *Entropy* **2022**, *24*, 1015.
- [36] A. Le Boité, M.-J. Hwang, H. Nha, M. B. Plenio, *Phys. Rev. A* **2016**, *94*, 033827.
- [37] A. Ridolfo, M. Leib, S. Savasta, M. J. Hartmann, *Phys. Rev. Lett.* **2012**, *109*, 193602.
- [38] Z.-M. Li, D. Ferri, D. Tilbrook, M. T. Batchelor, *J. Phys. A: Math. Theor.* **2021**, *54*, 405201.
- [39] M. Liu, Z.-J. Ying, J.-H. An, H.-G. Luo, *New J. Phys.* **2015**, *17*, 043001.
- [40] L. Cong, X.-M. Sun, M. Liu, Z.-J. Ying, H.-G. Luo, *Phys. Rev. A* **2017**, *95*, 063803.
- [41] L. Cong, X.-M. Sun, M. Liu, Z.-J. Ying, H.-G. Luo, *Phys. Rev. A* **2019**, *99*, 013815.
- [42] K. K. W. Ma, *Phys. Rev. A* **2020**, *102*, 053709.
- [43] Q.-H. Chen, C. Wang, S. He, T. Liu, K.-L. Wang, *Phys. Rev. A* **2012**, *86*, 023822 (2012).
- [44] L. Duan, Y.-F. Xie, D. Braak, Q.-H. Chen, *J. Phys. A* **2016**, *49*, 464002.
- [45] Y.-Y. Zhang, *Phys. Rev. A* **2016**, *94*, 063824.
- [46] Z. Lü, C. Zhao, H. Zheng, *J. Phys. A: Math. Theor.* **2017**, *50*, 074002.
- [47] M. T. Batchelor, H.-Q. Zhou, *Phys. Rev. A* **2015**, *91*, 053808.
- [48] Q. Xie, H. Zhong, M. T. Batchelor, C. Lee, *J. Phys. A: Math. Theor.* **2017**, *50*, 113001.
- [49] S. Bera, S. Florens, H. U. Baranger, N. Roch, A. Nazir, A. W. Chin, *Phys. Rev. B* **2014**, *89*, 121108(R).
- [50] L. Yu, S. Zhu, Q. Liang, G. Chen, S. Jia, *Phys. Rev. A* **2012**, *86*, 015803.
- [51] T. Liu, M. Feng, W. L. Yang, J. H. Zou, L. Li, Y. X. Fan, K. L. Wang, *Phys. Rev. A* **2013**, *88*, 013820.
- [52] J. Peng, E. Rico, J. Zhong, E. Solano, I. L. Egusquiza *Phys. Rev. A* **2019**, *100*, 063820.
- [53] J. Casanova, R. Puebla, H. Moya-Cessa, M. B. Plenio, *npj Quantum Information* **2018**, *4*, 47.
- [54] D. Braak, *Symmetry* **2019**, *11*, 1259.
- [55] V. V. Mangazeev, M. T. Batchelor, V. V. Bazhanov, *J. Phys. A: Math. Theor.* **2021**, *54*, 12LT01.
- [56] Z.-M. Li, M. T. Batchelor, *Phys. Rev. A* **2021**, *103*, 023719.
- [57] C. Reyes-Bustos, D. Braak, M. Wakayama, *J. Phys. A: Math. Theor.* **2021**, *54*, 285202.
- [58] J. Larson and T. Mavrogordatos, *The Jaynes-Cummings Model and Its Descendants*, IOP, London, **2021**.
- [59] L. Cong, S. Felicetti, J. Casanova, L. Lamata, E. Solano, I. Arrazola, *Phys. Rev. A* **2020** *101*, 032350.
- [60] A. L. Grimsmo, S. Parkins, *Phys. Rev. A* **2013**, *87*, 033814.
- [61] P. Forn-Díaz, J. Lisenfeld, D. Marcos, J. J. Garcia-Ripoll, E. Solano, C. J. P. M. Harmans, J. E. Mooij, *Phys. Rev. Lett.* **2010**, *105*, 237001.
- [62] A. Wallraff, D. I. Schuster, A. Blais, L. Frunzio, R.-S. Huang, J. Majer, S. Kumar, S. M. Girvin, R. J. Schoelkopf, *Nature* **2004**, 431, 162.
- [63] T. Niemczyk, F. Deppe, H. Huebl, E. P. Menzel, F. Hocke, M. J. Schwarz, J. J. Garcia-Ripoll, D. Zueco, T. Hümmer, E. Solano, A. Marx, R. Gross, *Nature Phys.* **2010**, *6*, 772.
- [64] G. Günter, A. A. Anappara, J. Hees, A. Sell, G. Biasiol, L. Sorba, S. De Liberato, C. Ciuti, A. Tredicucci, A. Leitenstorfer, R. Huber, *Nature* **2009**, *458*, 178.
- [65] P. Forn-Díaz, J. J. García-Ripoll, B. Peropadre, J. L. Orgiazzi, M. A. Yurtalan, R. Belyansky, C.M. Wilson, A. Lupascu, *Nat. Phys.* **2017**, *13*, 39.
- [66] B. Peropadre, P. Forn-Díaz, E. Solano, and J. J. García-Ripoll, *Phys. Rev. Lett.* **2010**, *105*, 023601.
- [67] G. Scalari, C. Maissen, D. Turčinková, D. Hagenmüller, S. De Liberato, C. Ciuti, C. Reichl, D. Schuh, W. Wegscheider, M. Beck, J. Faist, *Science* **2012**, *335*, 1323.
- [68] Z.-L. Xiang, S. Ashhab, J. Q. You, F. Nori, *Rev. Mod. Phys.* **2013**, *85*, 623. J.Q. You, F. Nori, *Phys. Rev. B* **2003**, *68*, 064509.
- [69] X. Gu, A. F. Kockum, A. Miranowicz, Y. X. Liu, F. Nori, *Phys. Rep.* **2017**, *718*, 1.
- [70] F. Yoshihara, T. Fuse, S. Ashhab, K. Kakuyanagi, S. Saito, K. Semba, *Nat. Phys.* **2017**, *13*, 44.
- [71] A. Bayer, M. Pozimski, S. Schambeck, D. Schuh, R. Huber, D. Bougeard, C. Lange, *Nano Lett.* **2017**, *17*, 6340.
- [72] I. I. Rabi, *Phys. Rev.* **1937**, *51*, 652.
- [73] K. Hepp, E. H. Lieb, *Ann. Phys.* **1973**, *76*, 360.
- [74] F. T. Hioe, *Phys. Rev. A* **1973**, *8*, 1440.
- [75] K. Baumann, C. Guerlin, F. Brennecke, T. Esslinger, *Nature* **2010**, *464*, 1301.
- [76] S. Sachdev, *Quantum phase transitions*, 2nd ed. Cambridge University Press, Cambridge, UK, **2011**.
- [77] When the critical universality collapses, the system properties are not unified any more but become diverse, see some illustrations and discussions in refs.^{19,21}.
- [78] M.-C. Gu, X.-G. Wen, *Phys. Rev. B* **1990**, *80*, 155131.
- [79] M. Z. Hasan, C. L. Kane, *Rev. Mod. Phys.* **2010**, *82*, 3045.

- [80] R. Yu, W. Zhang, H.-J. Zhang, S.-C. Zhang, X. Dai, Z. Fang, *Science* **2010**, *329*, 61.
- [81] W. Chen, A. P. Schnyder, *New J. Phys.* **2019**, *21*, 073003.
- [82] Z.-X. Li, Y. Cao, X.R. Wang, P. Yan, *Phys. Rev. Applied* **2020**, *13*, 064058.
- [83] H. Zou, E. Zhao, X.-W. Guan, W. V. Liu, *Phys. Rev. Lett.* **2019**, *122*, 180401.
- [84] Y. Che, C. Gneiting, T. Liu, F. Nori, *Phys. Rev. B* **2020**, *102*, 134213.
- [85] A. Amaricci, J. C. Budich, M. Capone, B. Trauzettel, G. Sangiovanni, *Phys. Rev. Lett.* **2015**, *114*, 185701.
- [86] C.-Z. Chen, J. Qi, D.-H. Xu, X.C. Xie, *Sci. China Phys. Mech. Astron.* **2021**, *64*, 127211.
- [87] a) M. Cohen, *Ph.D. Thesis*, California Institute of Technology **1956**; b) R. P. Feynman, M. Cohen, *Phys. Rev.* **1956**, *102*, 1189.
- [88] Y. Burda, *Ph.D. Thesis*, University of Toronto, Toronto, ON **2012**.
- [89] Y. Wang, W.-L. You, M. Liu, Y.-L. Dong, H.-G. Luo, G. Romero, J. Q. You, *New J. Phys.* **2018**, *20*, 053061.
- [90] E. T. Jaynes, F. W. Cummings, *Proc. IEEE* **1963**, *51*, 89.
- [91] X.-G. Wen, *Rev. Mod. Phys.* **2017**, *89*, 041004.
- [92] I. Pietikäinen, S. Danilin, K. S. Kumar, A. Vepsäläinen, D. S. Golubev, J. Tuorila, G. S. Paraoanu, *Phys. Rev. B* **2017**, *96*, 020501(R).
- [93] J. Casanova, G. Romero, I. Lizuain, J. J. García-Ripoll, E. Solano *Phys. Rev. Lett.* **2010** *105*, 263603.
- [94] J.-F. Huang, J.-Q. Liao, and L.-M. Kuang, *Phys. Rev. A* **2020**, *101*, 043835.
- [95] J. E. Mooij, T. P. Orlando, L. Levitov, L. Tian, C. H. van der Wal, S. Lloyd, *Science* **1999**, *285*, 1036.
- [96] F. Nagasawa, D. Frustaglia, H. Saarikoski, K. Richter, J. Nitta, *Nat. Commun.* **2013**, *4*, 2526.
- [97] Z.-J. Ying, P. Gentile, C. Ortix, M. Cuoco, *Phys. Rev. B* **2016**, *94*, 081406(R).
- [98] Z.-J. Ying, M. Cuoco, C. Ortix, P. Gentile, *Phys. Rev. B* **2017**, *96*, 100506(R).
- [99] Z.-J. Ying, P. Gentile, J. P. Baltanás, D. Frustaglia, C. Ortix, M. Cuoco, *Phys. Rev. Res.* **2020**, *2*, 023167.
- [100] P. Gentile, M. Cuoco, O. M. Volkov, Z.-J. Ying, I. J. Vera-Marun, D. Makarov, C. Ortix, *Nature Electronics* **2022**, *5*, 551.
- [101] Y.-J. Lin, K. Jiménez-García, I. B. Spielman, *Nature* **2011**, *471*, 83.
- [102] V. Galitski, Ian B. Spielman, *Nature* **2013**, *494*, 49.
- [103] Y. A. Bychkov, E. I. Rashba, *J. Phys. C* **1984**, *17*, 6039.
- [104] G. Dresselhaus, *Phys. Rev.* **1955**, *100*, 580.
- [105] Y. Li, L. P. Pitaevskii, S. Stringari, *Phys. Rev. Lett.* **2012**, *108*, 225301.
- [106] Before the dizzying painting factions including impressionism, post-impressionism, expressionism, cubism, fauvism, minimalism, abstractionism, modernism, surrealism, and so on and so forth, we didn't find ourselves until coming across the word radical "abstract" which we always have to deal with in all scientific papers.
- [107] Although in conventional classification of painting factions P. Picasso is the founder of cubism and a main representative of modernism, rather than abstractionism, we choose Picasso here as the iconic figure for the reason that we as laymen heard his name more, for which we hope the anisotropic QRM wouldn't mind.
- [108] P. Bertet, I. Chiorescu, C. J. P. M. Harmans, J. E. Mooij, *arXiv:cond-mat/0507290*.
- [109] J. Q. You, Y. Nakamura, Franco Nori, *Phys. Rev. B* **2005**, *71*, 024532.
- [110] A. Bermudez, M. A. Martin-Delgado, E. Solano, *Phys. Rev. A* **2007**, *76*, 041801(R).